ISSN 1063-7834, Physics of the Solid State, 2009, Vol. 51, No. 12, pp. 2505–2512. © Pleiades Publishing, Ltd., 2009.
Original Russian Text © K.S. Aleksandrov, S.V. Misyul, M.S. Molokeev, V.N. Voronov, 2009, published in Fizika Tverdogo Tela, 2009, Vol. 51, No. 12, pp. 2359–2364.

LATTICE DYNAMICS AND PHASE TRANSITIONS

Structures of Distorted Phases and Critical and Noncritical Atomic Displacements of Elpasolite Rb_2KInF_6 during Phase Transitions

K. S. Aleksandrov[a, b], S. V. Misyul[b, **], M. S. Molokeev[a, *], and V. N. Voronov[a]

[a] *Kirensky Institute of Physics, Siberian Branch, Russian Academy of Sciences, Akademgorodok, Krasnoyarsk, 660036 Russia*
* *e-mail: msmolokeev@mail.ru*
[b] *Siberian Federal University, pr. Svobody 79, Krasnoyarsk, 660041 Russia*
** *e-mail: misjul@akadem.ru*

Received February 4, 2009

Abstract—The structures of all three phases of the Rb_2KInF_6 crystal have been determined from the experimental X-ray diffraction data for the powder sample. The refinement of the profile and structural parameters has been carried out by the technique implemented in the DDM program, which minimizes the differences between the derivatives of the calculated and measured X-ray intensities over the entire profile of the X-ray diffraction pattern. The results obtained have been discussed using the group-theoretical analysis of the complete order-parameter condensate, which takes into account the critical and noncritical atomic displacements and permits the interpretation of the experimental data obtained previously. It has been reliably established that the sequence of changes in the symmetry during phase transitions in Rb_2KInF_6 can be represented as $Fm\bar{3}m \xrightarrow[0,0,\varphi]{11\text{-}9(\Gamma_4^+)} I114/m \xrightarrow[(\psi,\varphi,\varphi)]{11\text{-}9(\Gamma_4^+)\oplus 10\text{-}3(X_5^+)} P12_1/n1$.

PACS numbers: 61.05.cp, 63.70.+h, 61.50.Ks

DOI: 10.1134/S1063783409120130

1. INTRODUCTION

Crystals of $Rb_2KB^{3+}F_6$ series (B^3 = Fe, Sc, In, Lu, Y, Er, Ho, Dy, and Tb) have long been studied in connection with the investigation of the influence of sizes of B^3 ions on the sequence of phase transitions in them [1, 2]. All the above crystals belong to perovskite-like compounds with an elpasolite structure. The initial high-temperature phase G_0 of these crystals exhibits the symmetry $O_h^5 - Fm\bar{3}m$ ($Z = 4$), in which the fluorine octahedra $B^{3+}F_6$ and KF_6 alternate along the edges of the cubic cell, and the interoctahedral holes are occupied by the Rb ions.

Experimental [3–7] and theoretical [8] studies of these compounds have proved that the phase transitions in them are due to the instability with respect to the librational vibrations of octahedral groups. The group-theoretical analysis of lattice vibrations and the crystallographic analysis of the elpasolite structure [9–11] have demonstrated that the order parameters corresponding to the librational vibrations of the octahedra transform through irreducible representations $11\text{-}9(\Gamma_4^+)$ and $10\text{-}3(X_3^+)$ for the center, point Γ and boundaries, point X of the Brillouin zone of group $O_h^5 - Fm\bar{3}m$ (irreducible representations are denoted according to the handbooks [12, 13]). The distortions related to the condensation of the librational modes $11\text{-}9(\Gamma_4^+)$ and $10\text{-}3(X_3^+)$ are denoted in [10, 11] as distortions of the φ and ψ types, respectively. The irreducible representations and order parameters inducing changes in the symmetry are called critical or primary.

However, in some cases, the distortion of the initial-phase structure cannot be described using only critical order parameters. In a distorted (dissymmetric) phase, there can exist atomic displacements and orderings that are compatible with the symmetry of this phase and determined by the noncritical (secondary) order parameters and irreducible representations. The complete set of the critical and noncritical order parameters appearing during phase transitions forms a complete order-parameter condensate [14]. Recent studies [15, 16] on the group-theoretical analysis of the complete order-parameter condensate in the crystals with the initial phase $O_h^5 - Fm\bar{3}m$ showed that, in some phases, along with critical distortions of the φ and ψ types, noncritical distortions of the octahedral groups and noncritical displacements of atoms located in the interoctahedral holes should occur. Such displacements and distortions are of secondary character and insignificant near the phase transition points. The

Table 1. Main thermodynamic characteristics of Rb_2KInF_6 [4]

Characteristic	G_0	G_1	G_2
Phase transition temperature T_i, K	283	264	
Hysteresis of the phase transition temperature δT_i, K	–	0.92	
Change in the entropy $\Delta S/R$	0.18	0.59	
Space group	O_h^5–$Fm\bar{3}m$	C_{4h}^5–$I114/m$	C_{2h}^5–$P12_1/n1$
Number of formula units in the Bravais cell Z	4	2	2

symmetry analysis shows only the existence and type of noncrytical order parameters. However, the numerical values of both critical and noncritical distortions and order parameters participating in the complete condensate are found from experimental (primarily, structural) data.

The sequence of phase transitions in a Rb_2KInF_6 crystal was studied in [4] using polarization-optical, calorimetric, and X-ray diffraction methods. It was established in [4] that, as the temperature decreases, Rb_2KInF_6 undergoes two phase transitions, for which the temperatures and main thermodynamic characteristics are given in Table 1. Based on the experimental data, the following conclusions were drawn in [4]: (1) both phase transitions in Rb_2KInF_6 are displacive phase transitions, (2) the phase transition from the initial G_0 phase to the tetragonal G_1 phase is a second-order transition, the phase transition from the G_1 phase to the monoclinic G_2 phase is a first-order transition with a small thermal hysteresis, and (3) the distortions have a form (0, 0, φ) for the $G_0 \longrightarrow G_1$ phase transition and a form (ψ, φ, φ) for the $G_1 \longrightarrow G_2$ phase transition.

However, the inferences regarding the types of distortions in the phase transitions were made from indirect data, namely, from the temperature dependence of the crystal lattice parameters. Moreover, the temperature dependence of the superstructure reflections appearing in the monoclinic phase could not be explained only by rotations of the octahedral groups.

To answer the questions arisen, the structures of distorted phases should be determined directly. However, the determination of the structures of such phases in the Rb_2KInF_6 single crystals runs into a number of problems. The main problem is that, during phase transition, the crystal is twinned with a complex pattern of arrangement of the twins. For this reason, in the present work, the structures of all phases of the Rb_2KInF_6 crystal are determined using X-ray diffraction data experimentally obtained for the powder sample.

2. EXPERIMENTAL RESULTS

The transparent colorless Rb_2KInF_6 single crystal 9–11 mm in diameter and 10–15 mm long was grown by the Bridgman method in an evacuated sealed platinum ampoule. As the initial reagents, we used specially prepared RbF, KF, and $RbInF_4$ compounds taken in a stoichiometric ratio. The X-ray phase analysis showed the absence of excess phases in initial components and in the grown crystal. The powder sample for the X-ray diffraction studies was prepared from the single crystal.

The X-ray diffraction patterns of Rb_2KInF_6 were obtained using a TTK450 Anton Paar temperature-controlled camera mounted on a D8-ADVANCE diffractometer (CuK_α radiation, θ–2θ scan mode, VANTEC linear detector). Liquid nitrogen was used as a cooling agent. The scan step in the 2θ angle was equal to 0.016°, and exposure time at each point was 0.6 s. To exclude the influence of transition phenomena, sets of experimental data were measured at temperatures of 298, 270, and 143 K, i.e., fairly far from the phase transition temperature.

The refinement of the profile and structural parameters was carried out using a new procedure implemented in the DDM program which has not yet a wide application [17]. Unlike the Rietveld method [18], which is based on the use of the full profile of an X-ray powder diffraction pattern and minimizes the difference between the calculated and experimental intensities of the reflected X-ray radiation over the entire profile of the X-ray powder pattern, the DDM program minimizes the difference between values of the derivatives of the calculated and experimental intensities of the X-ray radiation. It gives a number of advantages as compared to the Rietveld method. First, it permits one to completely exclude the influence of the background on the process of refinement, since the background, which is a slowly oscillating function of the angle 2θ, has the derivative with respect to the angle 2θ close to zero. Second, the DDM program allows one to more correctly take into account the experimental intensities of the reflections located at large angles 2θ with intensities at the background level. As they are the reflections which are most sensitive to the values of the structural parameters, this opens a possibility to obtain more real values of the atomic coordinates and thermal factors. The DDM program and comparison of the results of refinement of the crystal structures

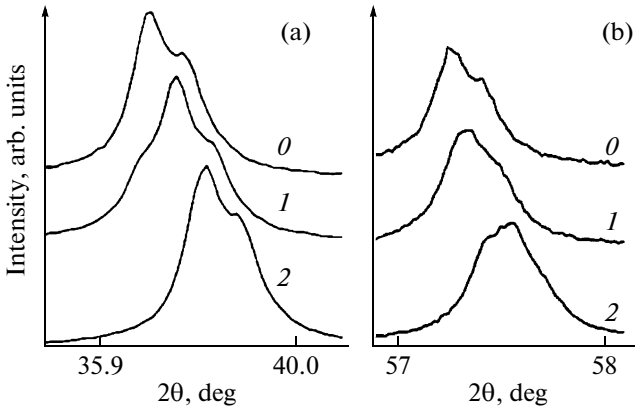

Fig. 1. Reflections in the X-ray powder diffraction patterns (CuK_α radiation) at experimental temperatures of (*0*) 298, (*1*) 270, and (*2*) 143 K: (a) (4, 0, 0) and (b) (4, 4, 0) reflections. The reflection indices are presented according to the parameters of the cubic Bravais cell.

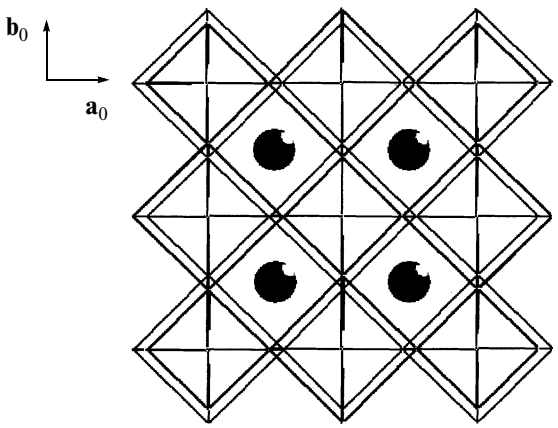

Fig. 2. Structure of the initial cubic phase of Rb_2KInF_6 at the temperature $T = 298$ K. Projection along the fourfold axis. Here and in Figs. 3 and 4, larger octahedra correspond to KF_6, smaller octahedra correspond to InF_6, and closed circles indicate the Rb ions.

obtained by the Rietveld and DDM methods are presented in detail in [19].

At the first stage of processing of the experimental data, the fitting procedure of the profile and shape of the X-ray diffraction peaks was performed. We determined also the shift of the X-ray diffraction patterns, which was 0.01°. The peak shape was described using the pseudo-Voigt function [19].

However, the reliable choice of space groups and determination of the values of the Bravais-lattice parameters from the experimental X-ray powder patterns were hampered at this stage because of faintly visible reflection splittings (Fig. 1) and low intensities of the superstructure reflections in the X-ray diffraction pattern of the monoclinic phase. Because of this, the above data were taken from [4], in which they were found from the X-ray diffraction experiment from the single-crystal Rb_2KInF_6 plates. Then, the parameters were refined in the course of processing of the X-ray diffraction experiment. Table 2 lists the main parameters of the data collection and refinement of the structure.

Table 2. Parameters of the data collection and refinement of the Rb_2KInF_6 structure

Parameter	Temperature of the experiment, K		
	298	270	143
Space group	O_h^5–$Fm\bar{3}m$	C_{4h}^5–$I114/m$	C_{2h}^5–$P12_1/n1$
a_i, Å	a_0, 9.09156(1)	$1/2(a_0 - b_0)$, 6.42098(1)	$1/2(a_0 - b_0)$, 6.3958(2)
b_i, Å	b_0, 9.09156(1)	$1/2(a_0 + b_0)$, 6.42098(1)	$1/2(a_0 + b_0)$, 6.4164(2)
c_i, Å	c_0, 9.09156(1)	c_0, 9.10056(3)	c_0, 9.0637(2)
β, deg	90	90	89.886(2)
Z	4	2	2
V, Å^3	751.48(1)	375.21(1)	371.96(2)
2θ, deg	7–110	7–110	7–110
Number of the Bragg reflections	40	129	468
Number of parameters refined	6	9	17
R_B, %	5.95	5.03	4.24
R_{DDM}, %	11.32	10.59	11.14

Note: R_B is the Bragg integral discrepancy factor, and R_{DDM} is the profile discrepancy factor determined with the DDM program [17, 19], which, as a rule, is larger than the discrepancy factor in the Rietveld method [18, 19]. The relationships between the Bravais-cell parameters of the initial G_0 and distorted G_i phases are presented.

Table 3. Coordinates, isotropic thermal parameters B_{iso}, anisotropic thermal parameters U_{ij}, and occupancies of the atomic positions p in the structures at temperatures of 298, 270, and 143 K

Atom	p	X	Y	Z	B_{iso}, Å^2; U_{ij}, Å^2
			$T = 298$ K		
Rb	1.0	0.25	0.25	0.25	3.49(4)
K	1.0	0.5	0.5	0.5	2.49(8)
In	1.0	0	0	0	2.08(2)
					7.8(2)
F	1.0	0.2242(4)	0	0	$U_{11} = 0.0031(7)$
					$U_{22} = U_{33} = 0.0354(7)$
			$T = 270$ K		
Rb	1.0	0	0.5	0.25	3.58(4)
K	1.0	0	0	0.5	2.33(9)
In	1.0	0.5	0.5	0.5	2.00(4)
F_1	1.0	0.307(2)	0.761(1)	0.5	3.5(3)
					20(1)
F_2	1.0	0	0	0.214(2)	$U_{11} = U_{22} = 0.098(7)$
				0.224*	$U_{33} = 0.04(4)$
			$T = 143$ K		
Rb	1.0	0	0.5259(2)	0.2535(6)	2.41(5)
K	1.0	0	0	0.5	1.50(9)
In	1.0	0.5	0.5	0.5	1.58(4)
F_1	1.0	0.241(3)	0.681(3)	0.534(2)	3.6(6)
F_2	1.0	0.062(3)	–0.013(1)	0.227(2)	0.5(5)
F_3	1.0	0.317(4)	0.231(3)	0.537(2)	3.5(6)

Note: The asterisk indicates the corrected coordinates of the F_2 atom.

At the second stage, the refinement of the atomic coordinates and thermal parameters was performed for the structures of all the phases.

In the initial cubic phase at 298 K, we refined six parameters: the coordinate x of the F atom, the isotropic parameters of the heavy atoms, and two anisotropic thermal parameters of the F atom (Table 3). The initial atomic coordinates in the distorted phases were found using the Patterson method. Then, the procedure of refining these coordinates together with the atomic thermal parameters was performed. In the tetragonal-phase structure at 270 K, the parameters of all the atoms, besides the F_2 atom located at the fourfold axis, were refined in the isotropic approximation. In the monoclinic phase, we localized all the atoms of the structure, including fluorine atoms F_1, F_2, and F_3 and refined their coordinates and thermal parameters using the isotropic approximation. The calculated results are given in Table 3. Table 4 lists selected bond lengths in the structures and the angles in the InF_6 octahedral group.

3. DISCUSSION OF THE RESULTS

Figures 2–4 depict the projections of the structures of all the phases of the Rb_2KInF_6 crystal. For convenience of comparison, the projections of the tetragonal and monoclinic phases are built along the coordinate axes of the initial cubic phase G_0. It follows from Tables 3 and 4 and Figs. 2–4 that, in the phase transition, the coordinates and thermal parameters of the F atoms are mainly changed. The thermal factors of the Rb, K, and In atoms are changed with temperature in the ordinary way. This is not true for the thermal parameters of the F atoms. In the cubic phase, the ellipsoids of thermal vibrations of F have a very flattened shape and are extended toward their subsequent displacements in the phase transition. As in chloride elpasolites [20], such a behavior is indicative of a substantial anharmonicity of the F-atom vibrations.

In the tetragonal G_1 phase, the F_1 atoms have an isotropic thermal factor which is half as large as that in the cubic phase. They are the atoms which are shifted during the phase transition from the cubic G_0 to tetrag-

Table 4. Selected bond lengths (Å) and angles (deg) in the InF_6 octahedron

Bond	$T = 298$ K	$T = 270$ K	$T = 143$ K
In–F_1	2.038(4)	2.08(1)	2.05(2)
In–F_2		1.95(1)/2.04*	2.10(2)
In–F_3			2.11(2)
K–F_1	2.508(4)	2.498(9)	2.58(2)
K–F_2		2.60(2)/2.51*	2.51(2)
K–F_3			2.53(2)
Rb–F_1	3.223(3)	3.011(7)	2.80(2)
Rb–F_2		3.227(2)/3.22*	2.82(2)
Rb–F_3			2.82(2)
Angle			
F_1–In–F_2	90	90.0(3)	91.0(5)
F_1–In–F_3	90	90	89.5(8)
F_2–In–F_3	90	90	91.1(5)

Note: The asterisks indicate the corrected distances.

Table 5. Angles of rotations φ and ψ (deg) of the InF_6 octahedra in the distorted phases at the experimental temperatures

Angle of rotation	Phase G_1 ($T = 270$ K)	Phase G_2 ($T = 143$ K)
φ	8	10
ψ	–	16
Symbol of distortions	(0, 0, φ)	(ψ, φ, φ)

Thus, the InF_6 octahedron rotations of the φ and ψ types are the critical order parameters in the phase transitions. Table 5 gives these parameters at the temperatures of the experiments. They transform by the irreducible representations 11-9(Γ_4^+) and 10-3(X_3^+). As shown in [15, 16], these critical irreducible representations are related to the noncritical irreducible representations 11-5(Γ_3^+) and 11-7(Γ_5^+). The nonorthogonal G_1 phase, participating in the distortions of the (0, 0, φ) type. The change in the thermal parameter of the F_2 atom which brings about a substantial displacement of F_2 in the direction of the In atom and distortion of the InF_6 octahedron is unusual.

To explain this fact, we refined the tetragonal phase in the absence of the F_2 atom and, then, constructed the difference electron density (Fig. 5). The maps of the difference electron density (Fig. 5) show that the real electron density related to the F_2 atom exhibits a complex shape and cannot be represented by an ellipsoid of revolution. Thus, the ellipsoid center does not coincide with the true position of the F_2 atom and is shifted by $\Delta \approx 0.09$ Å to the In atom (Fig. 6). Note that this atom is disordered in the tetragonal phase and, during the next phase transition to the monoclinic G_2 phase, is displaced from the position at the fourfold axis, participating in a total distortion (ψ, φ, φ). In Tables 3 and 4, the sign asterisk indicates the corrected coordinates and distances in which the F_2 atom is located.

It is worthy of notice the fact that the distortions of the octahedral groups (for definiteness, InF_6) from the regular shape are small in the G_1 and G_2 phases. Even in the monoclinic G_2 phase, the distortions from the ideal shape of the octahedron insignificantly exceed the standard deviations for the bond lengths and angles shown in the brackets in Table 4. Thus, as assumed previously in [4], both phase transitions in the Rb_2KInF_6 crystal are displacive phase transitions, and the changes in the symmetry in the distorted phases can be described by the InF_6 octahedron rotations.

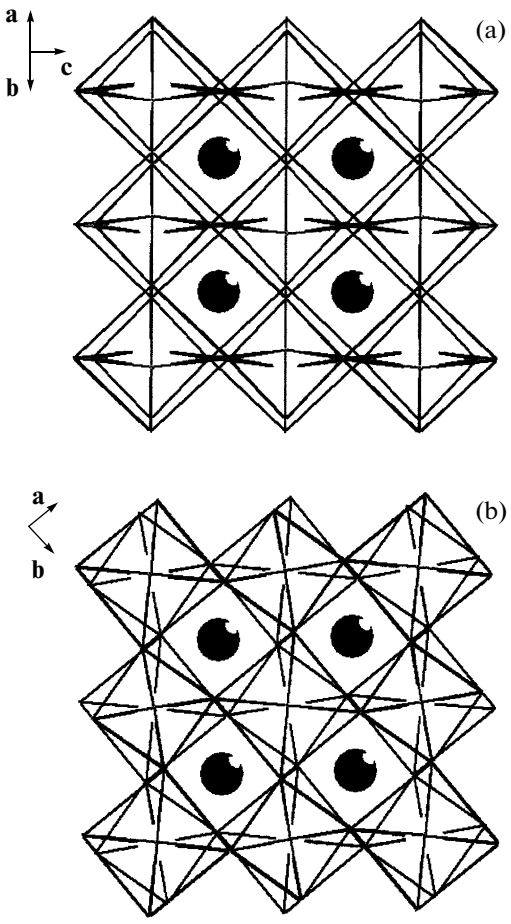

Fig. 3. Structure of the tetragonal phase of Rb_2KInF_2 at the temperature $T = 270$ K: (a) projection along the fourfold axis and (b) projection along the a_0 axis of the initial phase. The symbol of the distortion is (0, 0, φ).

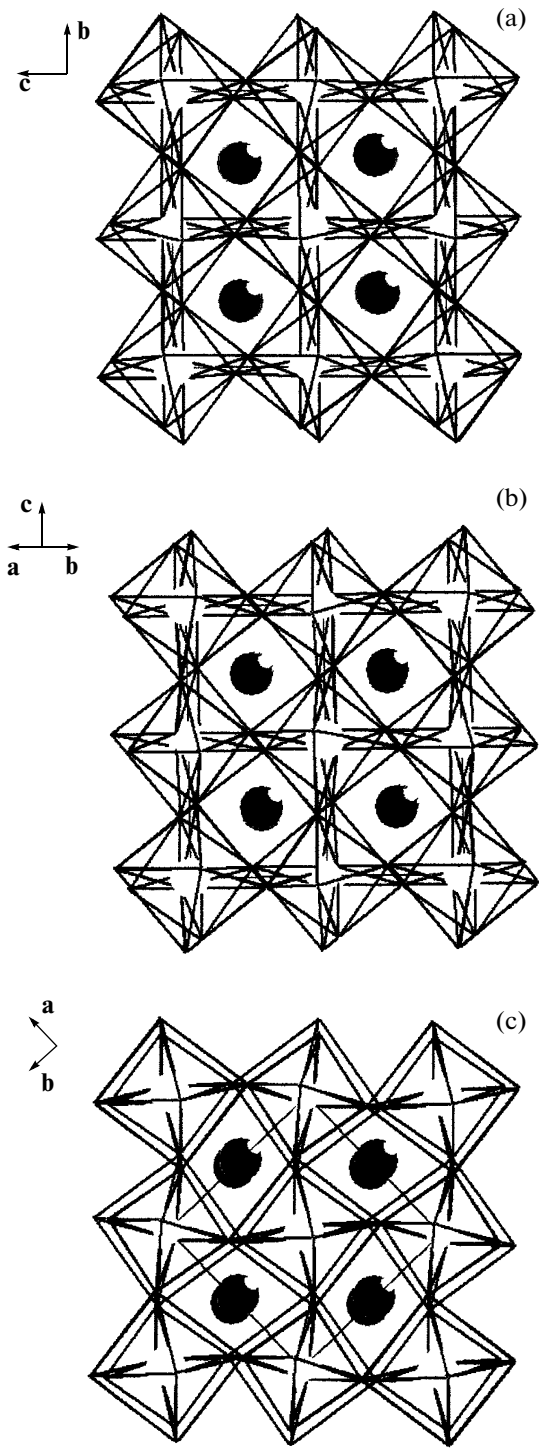

Fig. 4. Structure of the monoclinic phase of Rb_2KInF_2 at the temperature $T = 143$ K in projections (a) along the c_0 axis, (b) along the b_0 axis, and (c) along the a_0 axis of the initial cubic phase. The symbol of the distortion is (ψ, φ, φ).

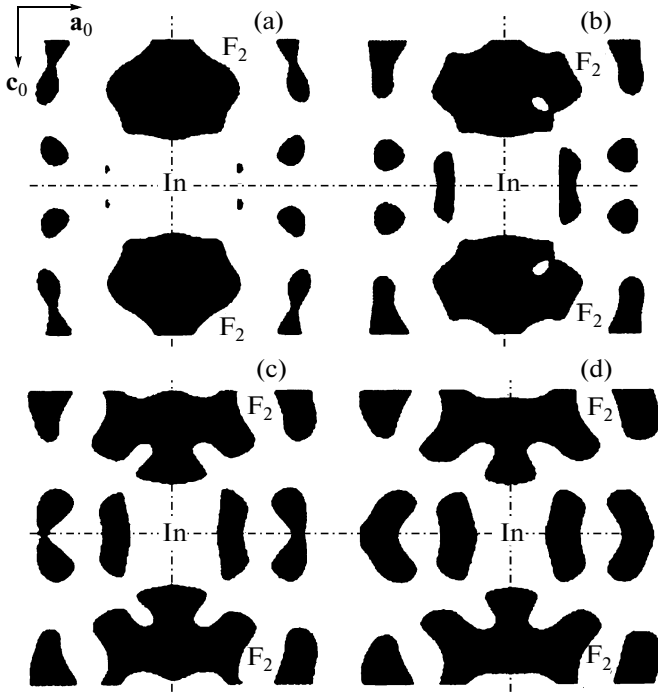

Fig. 5. Cross sections (perpendicular to the b_0 axis) of the difference electron density around the In atom in the tetragonal phase at $T = 270$ K: (a) cross section through the In atom and two F_2 atoms and (b–d) cross sections parallel to the cross section (a) with the shift along the b_0 axis by (b) 0.2, (c) 0.4, and (d) 0.6 Å.

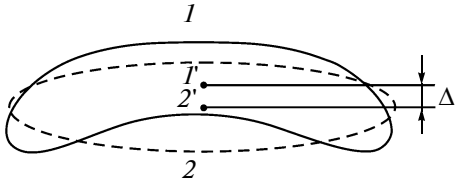

Fig. 6. Electron density around the F_2 atom: (*1*) real electron density ((*1*') is its center) and (*2*) ellipsoid of thermal vibrations of the F_2 atom ((*2*') is its center).

critical irreducible representation 11-5(Γ_3^+) insignificantly increases the In–F bond lengths in the $G_0 \longrightarrow G_1$ phase transition. In the $G_1 \longrightarrow G_2$ phase transition, already two irreducible representations 11-5(Γ_3^+) and 11-7(Γ_5^+) distort the InF_6 octahedron, and their integrated action to a greater degree distorts the octahedral groups (Table 4).

Now, we consider the displacement of the Rb atoms in the monoclinic phase. For example, in [21], based on the various experimental data, it was assumed that the phase transition in $Rb_2KB^{3+}F_6$ from the tetragonal to monoclinic phase can be due to the condensation of the 10-9(X_5^+) mode. In this case, the critical displacements can be not only the rotations of the $B^{3+}F_6$ octahedral groups but also the antiparallel displacements of the Rb atoms in the plane perpendicular to the rotation axis.

However, we assume that the librational vibrations 11-9(Γ_4^+) and 10-3(X_3^+) are most likely the critical vibrations in the phase transition in $Rb_2KB^{3+}F_6$. There are several reasons of such a choice.

First, it follows from the symmetry analysis of the lattice vibrations of the elpasolite structure [9, 10] that the 11-9(Γ_4^+)–10-3(X_3^+) branch in the Brillouin zone is a librational branch. Thus, if the $G_0 \longrightarrow G_1$ transition is due to the soft vibrations 11-9(Γ_4^+), a decrease in the 11-9(Γ_4^+) vibration frequency of the Brillouin-zone center brings about a lowering of the whole 11-9(Γ_4^+)–10-3(X_3^+) branch. Second, the first-principles calculations of the properties of a number of elpasolites with the general formula $Rb_2KB^{3+}F_6$ (see references in [8]) show that aforementioned modes are low-lying and most unstable in the Brillouin zone. Third, the significant value of the angle $\psi \approx 16°$ (Table 5) to a greater degree corresponds to the 10-3(X_3^+) librational vibration.

As indicated above, the noncritical irreducible representations 11-5(Γ_3^+) and 11-7(Γ_5^+) are related to the critical irreducible representations 11-9(Γ_4^+) and 10-3(X_3^+). Aside from the noncritical displacements of the F atoms, the displacements of the Rb atoms transform by the irreducible representation 11-7(Γ_5^+). As it follows from the analysis of the complete order-parameter condensate [15, 16], the displacements must differ by the value along the a_0, b_0, and c_0 axes of the initial G_0 phase. Comparing the Rb coordinates in the G_0 and G_2 phases at $T = 143$ K, we find that the Rb displacements are ~0.032 Å along the c_0 axis and ~0.118 Å along the a_0 and b_0 axes. Thus, the noncritical displacements of Rb along the a_0 and b_0 axes exceed the displacement along the c_0 axis by a factor of almost four. It is well seen in the projections of the monoclinic-phase structure (Fig. 4). Note that the data on the displacements were obtained at the temperature $T = 143$ K, i.e., lower by 121 K than the phase transition temperature $T_2 = 264$ K. Thus, despite of the fact that the Rb displacements are noncritical, they become significant at temperatures far from the phase transition temperature. Moreover, as the scattering power of the Rb atoms is substantially higher than that of the F atoms, their contribution to the intensity of the superstructure reflections is significant as well. These circumstances explain the temperature dependence of the superstructure reflections in the monoclinic G_2 phase.

4. CONCLUSIONS

The refined structures of the distorted phases clearly demonstrate that the critical distortions of the initial cubic elpasolite Rb_2KInF_6 structure are rotations of the InF_6 octahedral groups. However, to explain a set of experimental data, it is necessary to take into account the noncritical atomic displacements, which are reduced to insignificant distortions of the octahedra and displacements of the Rb atoms.

Thus, the whole sequence of the phase transitions in the Rb_2KInF_6 crystal can be symbolically represented as $Fm\bar{3}m \xrightarrow[0,\,0,\,\varphi]{\text{11-9}(\Gamma_4^+)} I114/m \xrightarrow[(\psi,\,\varphi,\,\varphi)]{\text{11-9}(\Gamma_4^+)\oplus\text{10-3}(X_3^+)} P12_1/n1$.

ACKNOWLEDGMENTS

This work was supported by the Council on Grants from the President of the Russian Federation, grant NSh-1011.2008.2.

REFERENCES

1. K. S. Aleksandrov and B. V. Beznosikov, *Perovskite-Type Crystals* (Nauka, Novosibirsk, 1997) [in Russian].
2. K. S. Aleksandrov and B. V. Beznosikov, *Perovskites: The Present and the Future (A Variety of Parent Phases, Phase Transitions, and Possibilities for Synthesis of New Compounds)* (Siberian Branch of the Russian Academy of Sciences, Novosibirsk, 2004) [in Russian].
3. I. N. Flerov, M. V. Gorev, S. V. Mel'nikova, S. V. Misyul', V. N. Voronov, and K. S. Aleksandrov, Fiz. Tverd. Tela (St. Petersburg) **34** (7), 2185 (1992) [Sov. Phys. Solid State **34** (7), 1168 (1992)].
4. I. N. Flerov, M. V. Gorev, S. V. Mel'nikova, S. V. Misyul', V. N. Voronov, K. S. Aleksandrov, A. Tressaud, J. Grannec, J.-P. Chaminade, L. Rabardel, and H. Guingard, Fiz. Tverd. Tela (St. Petersburg) **34** (11), 3493 (1992) [Phys. Solid State **34** (11), 1870 (1992)].
5. V. N. Voronov, M. V. Gorev, S. V. Mel'nikova, S. V. Misyul', and I. N. Flerov, Fiz. Tverd. Tela (Leningrad) **33** (10), 2945 (1991) [Sov. Phys. Solid State **33** (10), 1663 (1991)].
6. M. V. Gorev, I. N. Flerov, V. N. Voronov, and S. V. Misyul', Fiz. Tverd. Tela (St. Petersburg) **35** (4), 1022 (1993) [Phys. Solid State **35** (4), 524 (1993)].
7. H. Faget, J. Grannec, A. Tressaud, V. Rodriguez, T. Roisnel, I. N. Flerov, and M. V. Gorev, Eur. J. Solid State Inorg. Chem. **33**, 893 (1996).
8. E. G. Maksimov, V. I. Zinenko, and N. G. Zamkova, Usp. Fiz. Nauk **174** (11), 1145 (2004) [Phys.—Usp. **47** (11), 1075 (2004)].
9. S. V. Misyul', Kristallografiya **29** (5), 941 (1984) [Sov. Phys. Crystallogr. **29** (5), 554 (1984)].
10. K. S. Aleksandrov and S. V. Misyul', Kristallografiya **26** (5), 1074 (1981) [Sov. Phys. Crystallogr. **26** (5), 612 (1981)].

11. K. S. Aleksandrov and J. Bartolome, Phase Transform. **74**, 255 (2001).
12. O. V. Kovalev, *Irreducible and Induced Representations and Co-Representations of Fedorov's Groups* (Nauka, Moscow, 1986) [in Russian].
13. S. C. Miller and W. F. Love, *Tables of Irreducible Representations of the Space Groups and Co-Representations of Magnetic Space Groups* (Pruett, Boulder, Colorado, United States, 1967).
14. V. P. Sakhnenko, V. M. Talanov, and G. M. Chechin, Fiz. Met. Metalloved. **62**, 847 (1986).
15. E. E. Baturinets and S. V. Misyul', in *Proceedings of the Ninth International Symposium "Order, Disorder, and Properties of Oxides" (ODPO-2006), Rostov-on-Don, Russia, 2006* (Rostov-on-Don, 2006), p. 41.
16. K. S. Aleksandrov, S. V. Misyul, and E. E. Baturinets, Ferroelectrics **354**, 60 (2007).
17. L. A. Solovyov, J. Appl. Crystallogr. **37**, 1 (2004).
18. H. M. Rietveld, J. Appl. Crystallogr. **32**, 115 (1999).
19. L. A. Solovyov, A. M. Astachov, M. S. Molokeev, and A. D. Vasiliev, Acta Crystallogr., Sect. B: Struct. Sci. **61**, 435 (2005).
20. I. P. Makarova, S. V. Misjul, L. A. Muradyan, A. F. Bovina, V. I. Simonov, and K. S. Aleksandrov, Phys. Status Solidi B **121**, 481 (1984).
21. I. N. Flerov, M. V. Gorev, K. S. Aleksandrov, A. Tressaud, J. Grannec, and M. Couzi, Mater. Sci. Eng., R **24**, 81 (1998).

Translated by Yu. Ryzhkov